Feshbach-Kerman-Koonin analysis of ^{93}Nb reactions: $P \rightarrow Q$ transitions and reduced importance of multistep compound emission

M. B. Chadwick[1] and P. G. Young[2]
[1] *Nuclear Data Group, Lawrence Livermore National Laboratory, Livermore, California 94551*
[2] *Theoretical Division, Los Alamos National Laboratory, Los Alamos, New Mexico 87545*
(Received 23 November 1992)

We have implemented multistep compound (MSC) and multistep direct (MSD) preequilibrium theories of Feshbach, Kerman, and Koonin (FKK) for the calculation of nucleon-induced reactions. Unlike most previous analyses, which have concentrated on just one of these multistep mechanisms, we consider both mechanisms as well as subsequent Hauser-Feshbach equilibrium emission, and describe the complete nucleon emission spectra and angular distributions quantum mechanically. We compare theoretical calculations of (n,n') and (n,p) reactions on ^{93}Nb at energies of 14, 20, and 25.7 MeV with experimental data. Our analysis suggests that the FKK theory should be modified to allow transitions from the MSD to MSC preequilibrium chains, and shows MSC processes to be less important than previously thought. We find that the MSD mechanism dominates preequilibrium emission even for incident neutron energies as low as 14 MeV. A model to account for preequilibrium flux cascading from the MSD to MSC chain is presented, and we check its validity with a least-squares fit to data which establishes the experimentally observed partitioning between MSD and MSC.

PACS number(s): 24.60.Gv, 24.60.Dr, 25.40.Fq

I. INTRODUCTION

The quantum-mechanical preequilibrium theory of Feshbach, Kerman, and Koonin (FKK) [1] has been applied with considerable success to describe nucleon-induced reactions up to 200 MeV; see Refs. [2–4] for recent analyses. This theory describes the reaction as passing through a series of particle-hole excitations, caused by nucleon-nucleon interactions as the nuclear system evolves towards equilibrium. Preequilibrium emission occurs when particle decay takes place from simple particle-hole stages early in the reaction, and is typically of high energy and forward peaked. According to the FKK theory, two different types of preequilibrium emission can occur: multistep direct (MSD) and multistep compound (MSC). The majority of FKK analyses to date have concentrated on just one of these mechanisms and have analyzed restricted sets of experimental data with the assumption that only one of these two mechanisms is important. However, for most energy ranges both mechanisms are present.

In this paper we present FKK calculations which account for the whole emission spectrum of neutrons and protons, at all emission energies and angles, for neutron reactions on niobium. We show that it is necessary to perform MSD, MSC, and Hauser-Feshbach analyses concurrently to properly describe the reaction. In particular, we argue that MSC preequilibrium processes are less important than previously thought, and that there is considerable crossover from the MSD to MSC preequilibrium chains, in contradiction to the original FKK description of the reaction. These effects are difficult to establish unless one considers the whole emission spectrum for a number of incident energies. We have concentrated on niobium as an illustrative example since there exists a large amount of experimental data for its interaction with neutrons (due to interest in it by the fusion program). In a subsequent paper we shall present our FKK analyses of a large number of different target nuclei and incident energies.

Multistep direct reactions occur when at least one of the particles in the preequilibrium cascade is in the continuum (P space), whereas multistep compound processes occur when the excited particles in preequilibrium states are bound (Q space). FKK showed that the transition matrix elements in these two preequilibrium chains have very different statistical properties, resulting in MSD emissions having a forward-peaked angular distribution, and MSC emissions being symmetric about 90°. In general, MSD emission is most important for higher incident energies, and MSC emission for lower incident energies, though in almost all cases both mechanisms must be considered. Figure 1 shows the different

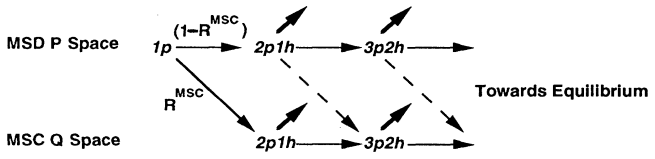

FIG. 1. Preequilibrium chains of unbound P space and bound Q space. Short arrows represent possible emission, and dashed arrows indicate $P \rightarrow Q$ transitions.

preequilibrium chains. The dashed lines indicate transitions from P to Q stages which we shall show to be important.

This research was motivated in part by the desire to use a quantum theory of preequilibrium reactions in nuclear data evaluation work, which usually relies on the semiclassical exciton or hybrid models. In Ref. [5] we described our code system FKK-GNASH, which enables the whole emission spectrum in a nucleon-induced reaction to be calculated quantum mechanically. There have been a number of other applications of quantum preequilibrium theories to describe ^{93}Nb reactions [3,4,6–9]. Our calculations differ from these works (except Ref. [9]) in that we describe the full emission spectrum (including multiple emission processes), and predict angular distributions for all emission energies. Angular distributions can be satisfactorily explained only with quantum theories, since distortion effects of the nucleon wave functions in the nuclear field are needed to account for backward-angle emission [10].

In Sec. II we describe the MSD theory, and in Sec. III the MSC and Hauser-Feshbach theories, along with various refinements to the original FKK formalism for calculating preequilibrium decay widths. We provide evidence for the existence of $P \rightarrow Q$ transitions beyond the initial $1p \rightarrow 2p1h$ (with p for particle and h for hole) transition in Sec. IV and present a model to account for the partitioning of the reaction flux between the P and Q chains. Our results are shown in Sec. V, where we compare theoretical calculations of (n,n') and (n,p) reactions on ^{93}Nb at incident neutron energies of 14, 20 and 25.7 MeV with experimental data. As a further test of our model for $P \rightarrow Q$ transitions, we perform a least-squares analysis of the experimental data in Sec. VI, using only the shapes of our calculated MSD and MSC spectra. Our conclusions are given in Sec. VII.

II. MULTISTEP DIRECT REACTIONS

MSD reactions occur when the P-space chain of states is populated (see Fig. 1), so that at least one particle is in the continuum. This particle maintains a "memory" of the initial direction of the projectile as it creates p-h states through scatterings with bound nucleons, and results in forward-peaked emission.

MSD theory represents an extension of distorted-wave-Born-approximation (DWBA) theory into the continuum, and can be derived from a Lippmann-Shwinger expansion of the transition amplitude [11]. The FKK theory differs from the theories of Tamura, Udagawa, and Lenske [12] and Nishioka, Weidenmuller, and Yoshida (NWY) [13] in the quantum-statistical assumptions concerning multiple-scattering processes, as discussed by Koning and Akkermans [11]. It has the advantage that random matrix element assumptions are made, allowing multiple-scattering processes to be expressed in terms of a convolution of single-step scattering cross sections. For the incident energies that we consider, only one- and two-step scattering needs to be included. The one-step cross section is given by

$$\left.\frac{d^2\sigma(E,\Omega \leftarrow E_0,\Omega_0)}{d\Omega\, dE}\right|_{\text{1-step}} = \sum_l (2l+1)\rho(1p,1h,E_0-E,l) \times \left\langle \left[\frac{d\sigma(E,\Omega \leftarrow E_0,\Omega_0)}{d\Omega}\right]_l^{\text{DWBA}} \right\rangle, \quad (1)$$

where l is the orbital angular momentum transfer, which equals the composite spin since we follow FKK in assuming spin-zero nucleons and target nucleus. $\rho(1p,1h,E_0-E,l)$ is the density of $1p1h$ states with energy E_0-E and spin l. In general the density of states for a p-particle, h-hole system can be partitioned into the energy-dependent density multiplied by a spin distribution, $\rho(p,h,E,l) = \omega(p,h,E)\ R_n(l)$. We use the Williams [14] equidistant expression

$$\omega(p,h,E) = \frac{g^n}{p!h!(n-1)!}(E-\Delta-A_{ph})^{n-1}, \quad (2)$$

where $n = p+h$, and we take the single-particle spacing as $g = A/13$ MeV^{-1}. The Pauli-blocking factor is $A_{ph} = [p^2+h^2+p-3h]/4g$, and the pairing energy corrections (Δ) of Dilg *et al.* [15] are used. A Gaussian angular momentum distribution is assumed,

$$R_n(l) = \frac{2l+1}{2\sqrt{2\pi}\sigma_n^3}\exp\left[-\frac{(l+1/2)^2}{2\sigma_n^2}\right], \quad (3)$$

with spin cutoff $\sigma_n^2 = 0.24nA^{2/3}$ [16].

$\left\langle \left[\frac{d\sigma(E,\Omega\leftarrow E_0,\Omega_0)}{d\Omega}\right]_l^{\text{DWBA}} \right\rangle$ is the average of DWBA cross sections exciting $1p1h$ states of energy E_0-E consistent with angular momentum and parity conservation. The $1p1h$ states are obtained from a spherical Nilsson model [17].

We follow Feshbach [18] in using DWBA matrix elements for the higher steps and obtain the two-step cross section as a convolution of one-step cross sections,

$$\left.\frac{d^2\sigma(E,\Omega \leftarrow E_0,\Omega_0)}{d\Omega\, dE}\right|_{\text{2-step}} = \frac{m}{4\pi^2\hbar^2}\int d\Omega_1 \int dE_1 E_1 \left.\frac{d^2\sigma(E,\Omega \leftarrow E_1,\Omega_1)}{d\Omega\, dE}\right|_{\text{1-step}} \left.\frac{d^2\sigma(E_1,\Omega_1 \leftarrow E_0,\Omega_0)}{d\Omega_1 dE_1}\right|_{\text{1-step}}. \quad (4)$$

It should be noted that our DWBA cross sections are obtained in a similar way to the calculations of Bonetti *et al.* [19] and Marcinkowski *et al.* [20], but not Koning and Akkermans [4]. We calculate the form factor for the various transitions with DWUCK4 [21] using a Yukawa potential of range 1 fm, and strength V_0, for $1p1h$ excitations. Koning and Akkermans, however, follow the prescription of Tamura, Udagawa, and Lenske [12] of replacing the average of many microscopic DWBA cross sections with just one fictitious collective state of deformation β_l, which

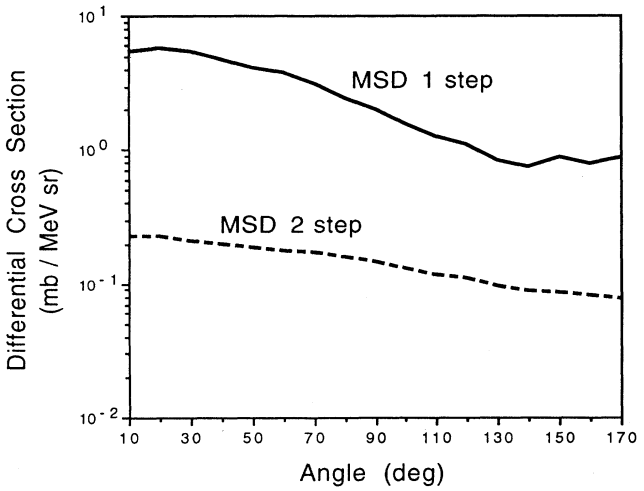

FIG. 2. One- and two-step MSD angular distributions for ^{93}Nb(n,n'), for an incident energy of 25.7 MeV and an emission energy of 12 MeV.

is treated as an adjustable parameter. Thus their deformation parameter β_l is analogous to our V_0 in affecting the overall magnitude of the MSD spectrum (which goes as V_0^2 for one step and V_0^4 for two step). With a CRAY computer we have no difficulty in averaging a large sample of microscopic $1p1h$ DWUCK4 cross sections (typically, for each 1 MeV energy bin, we average about five microscopic cross sections for each l transfer), and we believe this procedure is more in keeping with the FKK theory, which uses a particle-hole representation. We have found it important to include at least 12 values of l transfer in Eq. (1) to ensure that all possible $1p1h$ excitations are accounted for, and in (n,n') reactions we include microscopic form factors leading to both neutron p-h and proton p-h excitations. When calculating the form factors, unbound-state wave functions were obtained from optical-potential scattering states, and bound states from a real Woods-Saxon potential well with radius parameter 1.2 fm and diffuseness 0.6 fm. We apply a Gaussian smoothing to our calculated MSD cross sections of width 2 MeV, to remove artificial fluctuations which would not arise if we used deformed Nilsson single-particle states.

As an example of MSD cross sections, we show in Fig. 2 the one-step and two-step angular distributions for incident and emission energies of 25.7 MeV and 12 MeV, respectively, in the ^{93}Nb(n,n') reaction. The two-step contribution is much smaller than the one-step contribution, and less forward peaked, since the "memory" of the incident projectile direction is increasingly lost through successive nucleon-nucleon interactions. In addition to the forward peaking, the calculations show interference effects, leading to an increased cross section at the highest backward angles in one-step scattering. As seen in Sec. V of this paper, this effect is often observed in the data.

III. MULTISTEP COMPOUND REACTIONS

These occur when a chain of p-h states is populated in which all the particles are bound (the Q space of Fig. 1). The MSC contribution is greatest for low incident energies, becoming insignificant at high incident energies (above about 50 MeV), due to the decreasing probability of forming bound preequilibrium states with increasing energy. Matrix elements for MSC emission involving different total angular momenta, parity, and other quantum numbers are assumed to be random so that no interference terms remain on averaging, yielding angular distributions that are symmetric about 90°. Since our calculations show a negligible MSC deviation from isotropy [20], we obtain double-differential cross sections by evaluating the simpler differential cross section expression and dividing by 4π. We determine the amount of reaction flux into the MSC chain from a conventional optical model (reduced for MSD emission), and we allow this flux to enter the MSC chain at various stages along the chain, rather than all at the $2p1h$ stage [1]. The differential MSC cross section is given by

$$\frac{d\sigma}{dE} = \pi\lambda^2 \sum_J (2J+1)\,[R^{\mathrm{MSC}} T_J] \times \sum_{N=1}^{r} \sum_{\nu l} \frac{\langle \Gamma_{nJ}^{\uparrow \nu l}(U) \rangle}{\langle \Gamma_{nJ} \rangle} \prod_{M=1}^{N-1} \frac{\Gamma_{nJ}^{\downarrow}}{\Gamma_{nJ}}, \quad (5)$$

where $R^{\mathrm{MSC}} T_J$ is the transmission coefficient for producing bound $2p1h$ states of spin J, multiplied by a reduction factor R^{MSC} (discussed below) since only a fraction of the reaction flux enters this initial state. N labels each preequilibrium class, e.g., N=1 denotes $2p1h$, and n the number of excitons, $n = p + h = 2N + 1$. We include MSC emission from two preequilibrium stages before the equilibrium "r stage," since the ratio of emission to total MSC widths decreases strongly with increasing N. ν labels the three different emission modes corresponding to $\Delta n = 0, -2$, and $+2$ [1]. J and l denote the composite system spin and orbital angular momentum of the emitted particle, respectively. Following FKK, all nucleon spins are assumed to be zero, as are the spins of the target and residual nuclei. We showed in Refs. [3, 22] that this is a reasonable approximation. $\langle \Gamma_{nJ}^{\uparrow \nu l}(U) \rangle$ is the differential emission width for MSC preequilibrium decay of a nucleon with energy E, leaving a residual nucleus with energy U, described below. $\langle \Gamma_{nJ} \rangle$ is the total width of the MSC stage N, J, given by the sum of the damping width and the emission widths for neutron and proton emission. $\prod_{M=1}^{N-1} \Gamma_{nJ}^{\downarrow}/\Gamma_{nJ}$ is the depletion factor (again, $n = 2M+1$), accounting for the loss of MSC flux through emission from earlier preequilibrium stages.

Because the MSC preequilibrium stages have bound single-particle states, a two-body scattering process is needed for particle emission to occur. The emission and damping widths for a given preequilibrium state are calculated microscopically with a zero-range potential,

$$V(\mathbf{r}_1, \mathbf{r}_2) = V_0(\tfrac{4}{3}\pi r_0^3)\delta(\mathbf{r}_1 - \mathbf{r}_2), \quad (6)$$

where V_0 is the potential strength, and have the general form

$$\langle \Gamma_{nJ}^{\uparrow \nu l}(U) \rangle \text{ and } \langle \Gamma_{nJ}^{\downarrow} \rangle \sim X\,Y, \quad (7)$$

where X contains all the angular momentum coupling and the overlap integrals, and Y is the accessible phase space for the transition. We show below the expressions used for these functions.

A. X functions

For a given preequilibrium stage there are three emission X functions describing processes in which the number of excitons changes by 0, -2, and $+2$, and one damping X function. They are obtained by averaging the transition matrix element over initial states and summing over final states for a zero-range nucleon-nucleon interaction, and together they account for the angular momentum coupling in all possible decay channels. For simplicity we follow FKK in assuming spin-zero particles, since we showed in Ref. [3] that this is a good approximation. The emission X functions (where we have summed over the residual nucleus spin S), using the notation of Fig. 3, are [1]

$$X_{n\ J}^{\uparrow n\ l} = 2\pi \frac{(2l+1)}{R_n(J)}\ I_l^2 \sum_{Qj_3j_4} F(Q)(2j_3+1)\ R_1(j_3)R_{n-2}(j_4) \begin{pmatrix} l & j_3 & Q \\ 0 & 0 & 0 \end{pmatrix}^2 \Delta(QJj_4), \tag{8}$$

$$X_{n\ J}^{\uparrow n+2\ l} = 2\pi \frac{(2l+1)}{R_n(J)}\ I_l^2 \sum_{Qj_3j_4} R_1(Q)(2j_3+1)\ F(j_3)R_{n-1}(j_4) \begin{pmatrix} l & j_3 & Q \\ 0 & 0 & 0 \end{pmatrix}^2 \Delta(QJj_4), \tag{9}$$

$$X_{n\ J}^{\uparrow n-2\ l} = 2\pi \frac{I_l^2}{R_n(J)} \sum_S R_{n-3}(S)\Delta(lSJ) \left\{ \sum_{Qj_3} (2Q+1)F(Q)(2j_3+1)\ R_1(j_3) \begin{pmatrix} l & j_3 & Q \\ 0 & 0 & 0 \end{pmatrix}^2 \right\}, \tag{10}$$

and the damping X function is

$$X_{n\ J}^{\downarrow n+2} = 2\pi \frac{I_B^2}{R_n(J)} \sum_{Qj_3j_4\ l} (2l+1)\ R_1(l)R_1(Q)(2j_3+1)\ F(j_3)R_{n-1}(j_4) \begin{pmatrix} l & j_3 & Q \\ 0 & 0 & 0 \end{pmatrix}^2 \Delta(QJj_4), \tag{11}$$

where the triangular function $\Delta(abc)$ is defined as unity if $|a-b| \le c \le a+b$ and zero otherwise. We use the same Gaussian spin distribution function $R_n(J)$ and spin cutoff for MSC and MSD processes [see Eq. (3)]. The angular momentum density of a pair of states is given by

$$F(Q) = \sum_{j_1j_2} (2j_1+1)R_1(j_1)(2j_2+1)R_1(j_2) \begin{pmatrix} j_1 & j_2 & Q \\ 0 & 0 & 0 \end{pmatrix}^2. \tag{12}$$

The bound-continuum and bound-bound overlap integrals are obtained using the FKK assumption of constant wave functions [1],

$$I_l^2 = \frac{1}{2\pi}\frac{4}{3}\frac{V_0^2 r_0^3 k m T_l}{\hbar^3\ A}, \tag{13}$$

$$I_B^2 = \frac{V_0^2}{A^2}, \tag{14}$$

where k is the emitted momentum, T_l the transmission coefficient, A the nuclear mass, and r_0 the radius parameter, which we take to be 1.2 fm. It should be noted that I_l^2 contains the free phase space of the emitted particle. In previous works we determined overlap integrals using more realistic nuclear and scattering wave functions [3]. Such an approach runs into difficulties since it is often artificially sensitive to the choice of interacting states, and also the basis set of states needed for a realistic description is often larger than practically calculable. Thus, for application purposes, the original approach of FKK

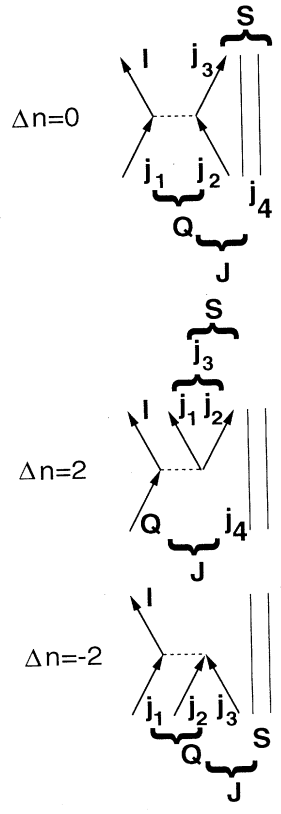

FIG. 3. Three X functions for $\Delta n = 0, 2$, and -2 processes. The angular momenta of individual components of the system are indicated in the diagrams.

is preferable. The MSC emission spectrum is independent of V_0, which cancels in the ratio of emission to total widths.

Neutron-proton distinguishability is accounted for in N=1 MSC emission by reducing a two-component formalism to a one-component formalism with correction factors applied to the escape widths. We find factors of 1.037 and 1.111 for Δn=0, 2, respectively, in (n,n') or (p,p') reactions, and 0.593, 0.888 for Δn=0, 2 in (n,p) or (p,n) reactions, obtained from Ref. [23] when the flux into the Q-chain $2p1h$ stage is set equal for one- and two-component approaches.

B. Y functions

It is essential that Y functions using only bound preequilibrium states are used when determining the accessible phase space for transitions. Such Y functions results in MSC emission spectra which differ considerably from those originally obtained by FKK. The three emission Y functions are given by [24]

$$Y_n^{\uparrow n}(U)=\frac{g^3}{\omega^B(p,h,E)}\left[\frac{\Theta(U-E+2B)}{2(n-2)}\left\{(U-E+2B)\omega^B(p-2,h,U^{n-2})+\frac{\omega^B(p-2,h,[E-2B]^{n-1})}{n-1}-\frac{\omega^B(p-2,h,U^{n-1})}{n-1}\right\}+B\frac{\omega^B(p-1,h-1,U^{n-2})}{n-2}\right], \tag{15}$$

$$Y_n^{\uparrow n+2}(U)=\frac{g^3}{2\omega^B(p,h,E)}\frac{\omega^B(p,h-1,U^n)}{n(n-1)}, \tag{16}$$

$$Y_n^{\uparrow n-2}(U)=\frac{\omega^B(p-2,h-1,U)}{\omega^B(p,h,E)}\omega^B(2,1,E-U), \tag{17}$$

for a residual nucleus energy of U. The damping Y function is given by

$$Y_n^{\downarrow}=\frac{g^4}{2\omega^B(p,h,E)}\left(\frac{\omega^B(p,h-1,E^{n+1})-\omega^B(p,h-1,[E-B]^{n+1})}{(n-1)n(n+1)}+\frac{\omega^B(p-1,h,E^{n+1})-\omega^B(p-1,h,[E-B]^{n+1})}{(n-1)n(n+1)}-B\frac{\omega^B(p-1,h,[E-B]^n)}{(n-1)n}-B^2\frac{\omega^B(p-1,h,[E-B]^{n-1})}{2(n-1)}\right). \tag{18}$$

In the above expressions the density of p-particle h-hole states is taken from an equidistant single-particle model, with the particles restricted to energies below the binding energy B,

$$\omega^B(p,h,E)=\frac{g^n}{p!h!(n-1)!}\sum_{i=0}^{p}(-1)^i\binom{p}{i}(E-\Delta-A_{ph}-iB)^{n-1}\Theta(E-\Delta-A_{ph}-iB), \tag{19}$$

where g,Δ and A_{ph} have the same meaning as in Eq. (2), and the theta function is unity if its argument is positive, and zero otherwise. In the above equations we also use the notation

$$\omega^B(p,h,E^{n+H})=\frac{g^n}{p!h!(n-1)!}\sum_{i=0}^{p}(-1)^i\binom{p}{i}(E-\Delta-A_{ph}-iB)^{n+H}\Theta(E-\Delta-A_{ph}-iB), \tag{20}$$

which should be used when the exponent $n+H \neq p+h-1$. This notation simplifies the analytic expressions for the Y functions which involve integrations of Eq. (19).

In Fig. 4 we show the emission Y functions for the first preequilibrium stage of the ^{93}Nb(n,n') reaction. For this N=1 stage, $\Delta n = -2$ processes are omitted since they correspond to elastic scattering. This Y-function dependence on emission energy carries over into the emission widths, resulting in Δn =2 processes being most important except for the highest emission energies, where Δn =0 dominates. The spin dependences of the N=1 and N=2 emission and damping preequilibrium widths are shown in Fig. 5. It is clear that the ratio of emission to damping width decreases strongly with increasing N, allowing us to consider only two preequilibrium stages and treat subsequent emission as being compound nucleus. When computing MSC emission cross sections the V_0^2 factors in the emission and damping widths cancel out.

C. "r-stage" or Hauser-Feshbach decay

Nuclei which do not undergo preequilibrium emission eventually become equilibrated and decay via compound nucleus emission. After calculating the primary MSD and MSC preequilibrium emission, we use the Hauser-Feshbach code GNASH [25] to describe the primary decay of compound nuclei that have survived preequilibrium decay, as well as the subsequent compound nucleus decay of residual nuclei remaining after preequilibrium and equilibrium particle emission.

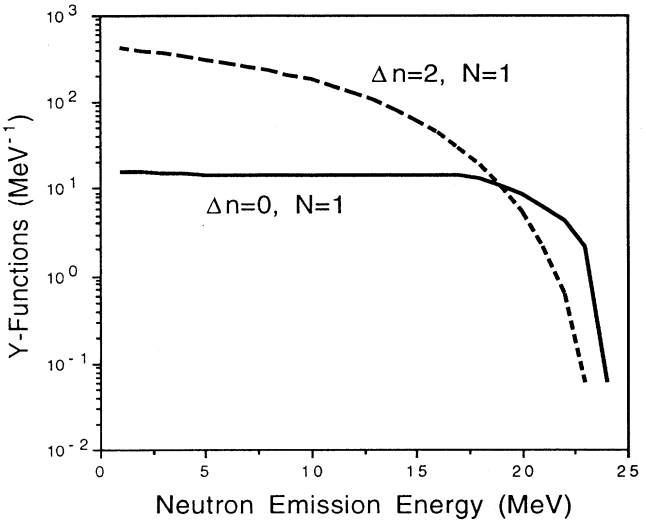

FIG. 4. Emission Y functions for N=1 neutron preequilibrium emission, for a 25.7 MeV induced ^{93}Nb(n,n') reaction.

The original FKK formulation calculated equilibrium emission using the "r-stage" formalism, which extended techniques used for calculating preequilibrium decay into the equilibrium regime, and FKK point out that formally it is very similar to Hauser-Feshbach theory. The relationship of r-stage decay and Hauser-Feshbach decay was considered in Ref. [24], and the differences shown to be small. Since Hauser-Feshbach theory has been so successful in describing compound nucleus decay, we use it, rather than the r-stage approach. This allows us to use the GNASH code system, which readily calculates all possible emission channels of all residual nuclei and includes photon competition in decay sequences. The contribution from multiparticle reactions to neutron and proton emission spectra can be substantial at lower emission energies.

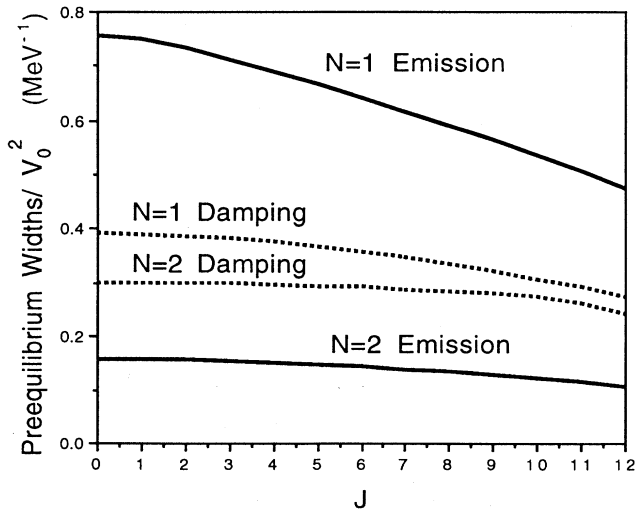

FIG. 5. Spin dependence of the N=1 and N=2 MSC emission and damping widths for a 26 MeV induced ^{93}Nb(n,n') reaction.

IV. MODIFICATION TO FKK: $P \rightarrow Q$ TRANSITIONS

Here we present a modification to the FKK theory which must be made in order to obtain a satisfactory description of data. Our modification leads to an increased stress on MSD processes, to diminishing importance of MSC processes, and to the feature of $P \rightarrow Q$ transitions, which were discounted by FKK. The need for $P \rightarrow Q$ transitions (beyond the initial $1p \rightarrow 2p1h$) in the FKK theory was first pointed out in Ref. [22], and has since been discussed in a number of works, e.g., Refs. [9, 26]. Herman has also stated the need for this phenomena when applying the NWY multistep theory [27]. While a theoretical formalism describing $P \rightarrow Q$ transitions has been suggested [28], we show how a detailed understanding of such mechanism is unnecessary in practical calculations, and that a requirement of unitarity is sufficient to describe these processes.

In the original FKK picture of the reaction, the incident flux splits immediately at the first interaction into the P and Q chains. Since, for example, 14 MeV reactions typically exhibit about 10% of primary emission which is forward peaked, it was assumed that 90% of the reaction flux entered the Q chain at the initial $2p1h$ stage. However, improvements to MSC calculations (specifically, the improved Y functions) lead to much more MSC emission for a given population of Q states than FKK originally calculated. The consequence is that if one allows 90% of the reaction flux to enter the Q chain at the initial $2p1h$ stage, far too much MSC preequilibrium emission occurs, overpredicting the data.

Historically, the omission of $P \rightarrow Q$ transitions also has some other origins. First, it is only recently that we have developed the capability to calculate MSD as well as MSC emission, and unless one attempts to describe the whole emission spectrum (and angular distributions), it is easy to miss this effect. Most earlier analyses isolated one part of the spectrum, and assumed that only MSC, or only MSD, emission is important. As an example, it has been frequently assumed that MSD emission is insignificant at backward angles, allowing a comparison of MSC calculations with backward-angle data [1, 3, 8]. Our results show this to be in error, because MSD emission, while forward peaked, still contributes relatively strongly at back angles. Second, we think that FKK overstated the case in claiming that "the experimental angular distributions are symmetric about 90°" when referring to Grimes' (p,n) data. At the higher emission energies this is not so, and consequently the role of MSC emission was probably overemphasized.

If the fraction of reaction flux entering the Q chain at the $2p1h$ stage, R^{MSC}, is reduced, and flux is allowed to cascade from $P \rightarrow Q$ states at later stages in the reaction (see dashed arrows in Fig. 1), then the amount of MSC emission is reduced, but the fraction of symmetric primary emission can still be maintained at the required (usually large) level. This is so because preequilibrium emission from stages more complex than $2p1h$ is relatively insignificant. In accordance with statistical ideas usually used in the exciton model, we can estimate the

fraction of flux into the initial $2p1h$ Q stage (at an energy E) as

$$R^{\rm MSC} = \frac{\omega^B(2p,1h,E)}{\omega(2p,1h,E)}, \tag{21}$$

i.e., the ratio of bound to total $2p1h$ phase space, calculated with the restricted and unrestricted Williams expressions, Eqs. (19) and (2). For the energies considered here, this becomes

$$R^{\rm MSC} = 2\left(\frac{B}{E}\right)^2. \tag{22}$$

This statistical division is consistent with the FKK picture of a partitioning of bound and unbound states, and is expected to yield reasonable results since the Kalbach systematics [29] make a similar assumption about the MSD/MSC division, and yield very reasonable angular distributions. Also, theoretical calculations [22] of the entrance strength function to the bound $2p1h$ stage indicate a small $R^{\rm MSC}$ compatible with Eq. (21). As shown in Fig. 1, we expect the $P\rightarrow Q$ transitions to occur predominantly via $\Delta n = +2$ processes due to the higher accessible phase-space, and also phase-space arguments indicate that $P\rightarrow Q$ transitions should be very likely. It would be possible to apply the same kind of reasoning as in Eq. (21), extended to more complex stages, to determine the $P\rightarrow Q$ flux for different preequilibrium stages. But since the probability of MSC emission is so insignificant for stages beyond the $2p1h$, in practice the exact details of this mechanism are not important, and it can be assumed that all the $P\rightarrow Q$ flux eventually decays by Hauser-Feshbach emission.

Our calculational procedure is therefore entirely well defined: (1) Calculate MSC emission, using Eq. (21). There are no free parameters. (2) To determine the MSD spectrum, consider angle-integrated data at a high emission energy where Hauser-Feshbach decay is insignificant, but below the energies where collective effects appear. V_0, and hence the MSD spectrum, is determined by equating MSD emission with the difference between data and MSC emission. (3) Calculate collective effects using the approach of Kalka, Torjman, and Seeliger [30] or coupled channels. (4) Calculate Hauser-Feshbach emission with GNASH. Unitarity requires that the flux available for primary Hauser-Feshbach decay be $\sigma_{\rm HF} = \sigma_R - \sigma_{\rm MSD} - \sigma_{\rm MSC}$, σ_R being the reaction flux. This implicitly accounts for $P\rightarrow Q$ transitions and assumes (reasonably) that preequilibrium decay following such transitions is negligible. Calculate subsequent equilibrium decay of all residual nuclei. (5) We take the residual nucleus spin distribution after preequilibrium emission from the Hauser-Feshbach spin distribution calculation, and we assume that MSC and Hauser-Feshbach emissions are isotropic.

V. RESULTS

We have analyzed experimental data for neutron-induced reactions on ^{93}Nb at 14, 20, and 25.7 MeV. All these sets of data exhibit clear signs of preequilibrium emission, and it represents a strong test of theory to be able to describe experiment for a range of incident energies and emission channels. The input parameters for our Hauser-Feshbach calculation were the standard ones used by GNASH in Ref. [31], with the exception that the level-density parameter for ^{93}Zr was reduced to $a = 10.75$ MeV^{-1}. The Wilmore-Hodgson optical potential [32] was used for neutrons, and the Becchetti-Greenlees potential [33] for protons. Direct collective effects were calculated using the approach of Kalka, Torjman, and Seeliger, with a real potential depth of 48 MeV and a radius parameter of 1.4 fm [30].

Figures 6 and 7 show our 14 MeV angle-integrated spectra compared with Vonach's evaluated ^{93}Nb(n,n') and (n,p) data. The same MSD residual interaction strength V_0=39.3 MeV was used for both the (n,n') and (n,p) channels, and it is evident that we obtain a very reasonable description of data. Perhaps even more importantly, the angular distributions for these two reactions, shown in Figs. 8 and 9, are accounted for reasonably well by our calculations. Our approach has significantly less MSC emission than the FKK analyses of Refs. [3, 6] or the NWY analysis of [8] [which did not include MSD and concentrated only on (n,n') backward-angle data]. This is because our MSD contribution, while forward peaked, still contributes significantly at back angles (see Figs. 8 and 9). If the amount of MSC emission we obtain were too small, this deficiency would be manifested in theoretical angular distributions which would be too forward peaked. But this is not the case, and our angular distributions have about the correct forward peaking. This is the first time that the FKK MSD theory has been applied at 14 MeV, and we find much more MSD emission than has previously been thought [3,6]. As mentioned earlier, this is a consequence of the fact that much of the observed backward-angle emission, which was previously assumed to arise solely from MSC emission, can be accounted for by MSD emission.

In Figs. 10 and 11 we compare our calculations with the 20 and 25.7 MeV induced ^{93}Nb(n,n') data of Marcinkowski *et al* [9]. The 25.7 MeV reaction was the

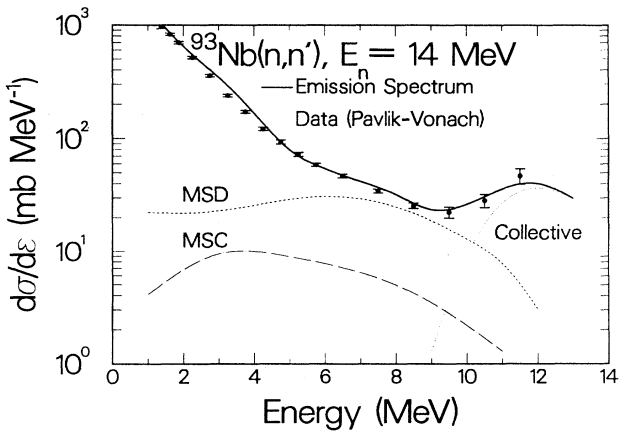

FIG. 6. FKK-GNASH calculated spectrum compared with data [34] for 14 MeV ^{93}Nb(n,n').

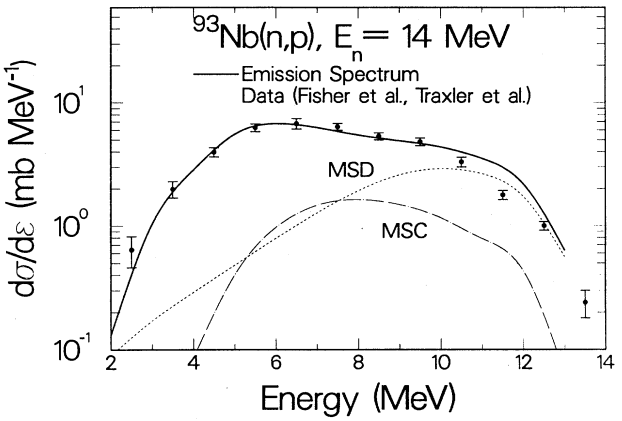

FIG. 7. FKK-GNASH calculated spectrum compared with data [35] for 14 MeV ^{93}Nb(n,p).

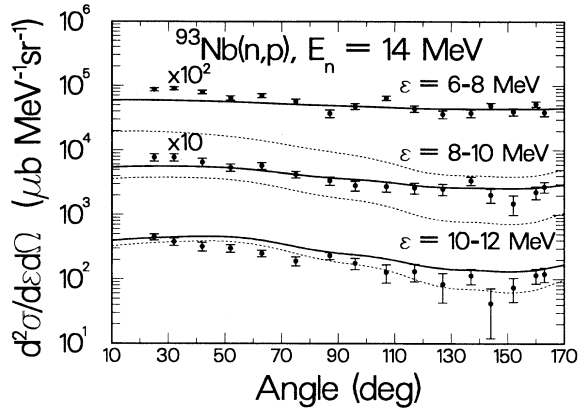

FIG. 9. FKK-GNASH angular distributions compared with data [35] for 14 MeV ^{93}Nb(n,p). The dashed line is solely MSD emission, and the solid line includes MSC and Hauser-Feshbach emission.

focus of an intercomparison of semiclassical codes [31], and the 20 and 25.7 MeV reactions have been analyzed by Marcinkowski *et al.* [9] and Koning and Akkermans [4], respectively. We use MSD residual interaction strengths of V_0=33.6 and 27.3 MeV, respectively, for the 20 and 25.7 MeV reactions, and again the description of the data is quite good, though it appears that our MSD strength falls off too rapidly at the highest energies resulting in an underprediction of data at energies just below the region of collective enhancement. Preliminary calculations indicate that this deficiency is removed if we use a deformed Nilsson single-particle scheme. Also, the collective-excitation peak at high neutron emission energies is seen to be described well by the theory of Kalka, Torjman, and Seeliger [30] for the 14 MeV reaction, but is underpredicted for the 20 and 25.7 MeV reactions. This reflects the fact that this component of the data does not follow the usual inverse proportionality to the incident energy. Figures 12 and 13 compare our predicted angular distributions with data for the 20, and 25.7 MeV

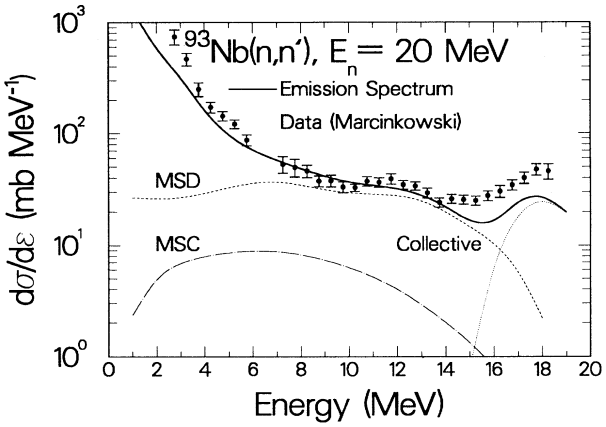

FIG. 10. FKK-GNASH calculated spectrum compared with data [9] for 20 MeV ^{93}Nb(n,n').

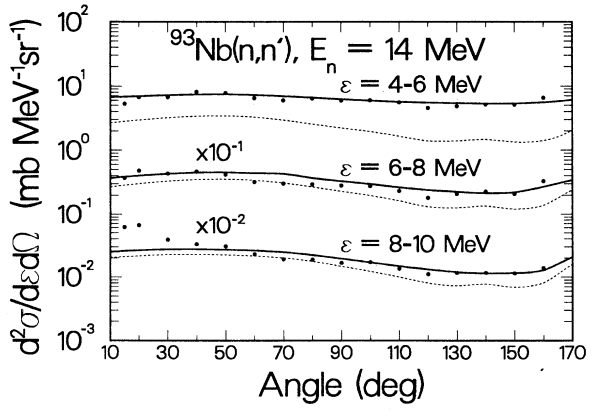

FIG. 8. FKK-GNASH angular distributions compared with data [36] for 14 MeV ^{93}Nb(n,n'). The dashed line is solely MSD emission, and the solid line includes MSC and Hauser-Feshbach emission.

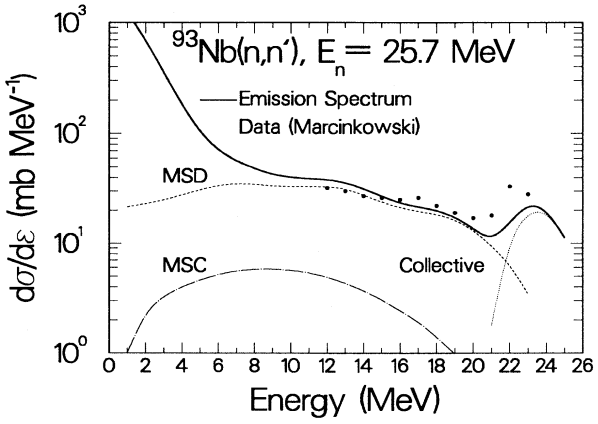

FIG. 11. FKK-GNASH calculated spectrum compared with data [37] for 25.7 MeV ^{93}Nb(n,n').

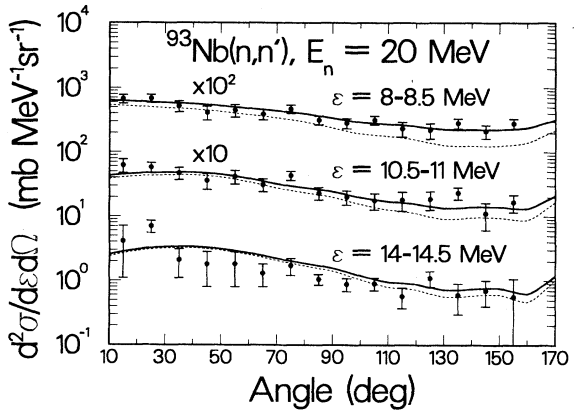

FIG. 12. FKK-GNASH angular distributions compared with data [9] for 20 MeV ^{93}Nb(n,n'). The dashed line is solely MSD emission, and the solid line includes MSC and Hauser-Feshbach emission.

reactions. Unlike semiclassical approaches, which underpredict backward-angle emission, we are able to describe the angular distributions well.

In our analysis the MSD effective interaction strength V_0 is the only free parameter. Our extracted values shown above follow approximately a $V_0^2 \propto 1/E_{\rm inc}$ variation, which was also found by Koning [38] (for his β_l parameter), and which is reminiscent of the usual matrix-element parametrization of the semiclassical exciton model [39]. Our value of $V_0 = 27.3$ MeV at $E_{\rm inc}$=25.7 MeV is in good agreement with values extracted from other MSD analyses [26], though for lower incident energies our extracted values exceed the parametrization in Ref. [26]. However, our calculation is the first MSD analysis at an energy as low as 14 MeV. An important area of future work is to compare our calculations with data for a wide range of target nuclei and incident energies to establish the systematics of V_0.

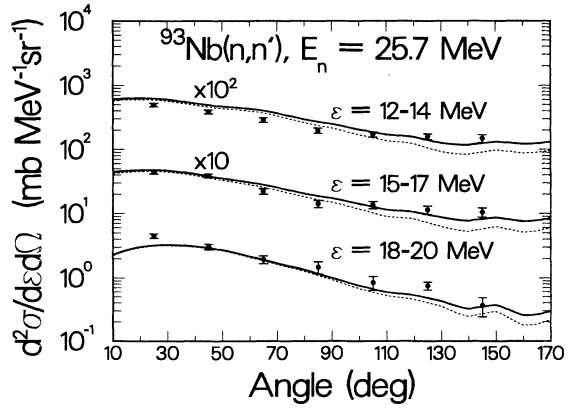

FIG. 13. FKK-GNASH angular distributions compared with data [37] for 25.7 MeV ^{93}Nb(n,n'). The dashed line is solely MSD emission, and the solid line includes MSC and Hauser-Feshbach emission.

VI. STATISTICAL ANALYSIS — CHECK OF $P \rightarrow Q$ MODEL

Experimental double-differential cross sections can be analyzed to determine relative contributions of MSC and MSD emissions, facilitating a quantitative check of our approach. The relative contributions of MSC and MSD emissions affect the extent of forward peaking in our calculated angular distributions. While the calculated shapes appear to have about the correct shape when compared "by eye" with the angular distribution data, a more rigorous check is useful. This is possible since we have calculated the shape of the MSD angular distribution, and the MSC shape is known to be essentially isotropic. The double-differential emission cross can be expressed as

$$\frac{d^2\sigma}{dE\,d\theta} = a\frac{d^2\sigma}{dE\,d\theta_{\rm MSD}} + b\frac{d^2\sigma}{dE\,d\theta_{\rm MSC}} + \frac{d^2\sigma}{dE\,d\theta_{\rm HF}}, \qquad (23)$$

where a and b describe the relative amounts of MSD and MSC emissions. The Hauser-Feshbach cross section $d^2\sigma/dE\,d\theta_{\rm HF}$ is insensitive to the partitioning of the preequilibrium flux between MSD and MSC emissions, and hence we subtract our calculated Hauser-Feshbach cross section from the experimental data, and then perform a least-squares analysis on the "corrected" data (which now accounts for only preequilibrium processes) to establish a and b. This approach enables us to estimate from the data what $R^{\rm MSC}$ should be (i.e., what fraction of the reaction flux enters the initial $2p1h$ Q state), with the only assumption being that we trust the *shapes* of our calculated MSD and MSC cross sections.

We have performed such an analysis for the above reactions for the data sets shown in Figs. 8, 12, and 13, obtaining results for $R^{\rm MSC}$ as shown in Fig. 14. We

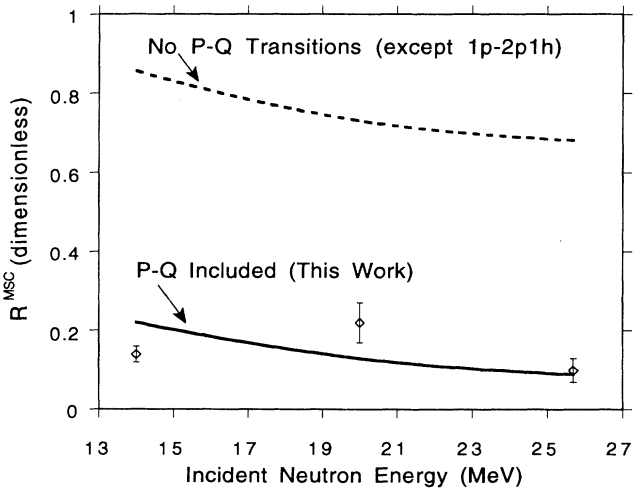

FIG. 14. Experimentally extracted values of $R^{\rm MSC}$ from a least-squares analysis of data, compared with our present model [solid line; see Eq. (21)], and the results that follow if $P \rightarrow Q$ transitions are ignored beyond $1p \rightarrow 2p1h$ (dashed line). The latter are not unity since flux is lost to MSD emission.

also show the values of R^{MSC} used in this analysis calculated theoretically from Eq. (21), and those that result when $P \rightarrow Q$ transitions are not included. Our theoretical model for R^{MSC} is seen to account for the data rather well, though there are some differences. However, the error bars on the experimentally extracted R^{MSC} values are probably too small since they assume that the Hauser-Feshbach cross sections and the MSD and MSC shapes are known exactly. It is clear, though, that if $P \rightarrow Q$ transitions are not included, the values obtained for R^{MSC} are completely inconsistent with experimental data. This provides strong evidence for the existence of these processes (which make up about 60% of the reaction cross section at 14 MeV), and shows that our model for obtaining R^{MSC} [Eq. (21)] is fairly accurate.

Since Feshbach, Kerman, and Koonin [1] presented their theory of MSC reactions, a number of papers aimed to show the presence of MSC effects in nucleon-induced reactions below 20 MeV [3, 6, 40]. We have argued here that MSC emission is less important than these papers suggested, and that these misinterpretations [including those of one of the present authors (M.B.C.)] resulted from the lack of MSD calculations. However, it should be emphasized that our least-squares analysis provides strong evidence for the existence of MSC reactions: The high-energy preequilibrium angular distribution data clearly show a symmetric component in addition to the forward-peaked MSD emission.

VII. CONCLUSIONS

We have shown that the FKK theory gives a very satisfactory description of preequilibrium reactions, provided it is modified to allow $P \rightarrow Q$ transitions. The importance of such crossover transitions can be most clearly seen when FKK analyses are compared with data for the whole emission spectrum and angular distributions. We suggested a model to account for these transitions based on phase-space arguments, and used a least-squares analysis to show that it describes experiment fairly well for incident neutron energies between 14 and 25.7 MeV on ^{93}Nb. Our analyses indicate that the MSD mechanism dominates preequilibrium emission even for energies as low as 14 MeV. The commonly made assumption that MSD emission can be ignored at backward angles (for 10–20 MeV reactions) is incorrect. This assumption, of course, was made in the past in the absence of any MSD calculations.

ACKNOWLEDGMENTS

We would like to thank Dr. S.M. Grimes, Dr. M. Herman, Dr. P.E. Hodgson, Dr. A. Kerman, Dr. A. Koning, Dr. A. Marcinkowski, Dr. D. Muir, Dr. D. Olaniyi, Dr. S. Yoshida, and Professor H. Vonach for helpful discussions. This work was performed under the auspices of the U.S. Department of Energy by the Lawrence Livermore National Laboratory under Contract No. W-7405-ENG-48.

[1] H. Feshbach, A. Kerman, and S. Koonin, Ann. Phys. (N.Y.) **125**, 429 (1980).
[2] W.A. Richter, A.A. Cowley, R. Lindsay, J.J. Lawrie, S.V. Fortsch, J.V. Pilcher, R. Bonetti, and P.E. Hodgson, Phys. Rev. C **46**, 1030 (1992).
[3] R. Bonetti, M.B. Chadwick, P.E. Hodgson, B.V. Carlson, and M.S. Hussein, Phys. Rep. **202**, 171 (1991).
[4] A.J. Koning and J.M. Akkermans, Phys. Rev. C **47**, 724 (1993).
[5] M.B. Chadwick and P.G. Young, in *Proceedings of the Symposium on Nuclear Data Evaluation Methodology*, Brookhaven National Laboratory, Upton, New York, 1992, edited by C. Dunford (World Scientific, Singapore, in press); Los Alamos Report No. LA-UR-93-104, 1993.
[6] M. Herman, A. Marcinkowski, and K. Stankiewicz, Nucl. Phys. **A430**, 69 (1984).
[7] H. Kalka, D. Seeliger, and F.A. Zhivopistsev, Z. Phys. A **329**, 331 (1988).
[8] M. Herman, G. Reffo, and H.A. Weidenmuller, Nucl. Phys. **A536**, 124 (1992).
[9] A. Marcinkowski, J. Rapaport, R. Finlay, X. Aslanoglou, and D. Kielan, Nucl. Phys. **A530**, 75 (1991).
[10] M.B. Chadwick and P. Oblozinsky, Phys. Rev. C **46**, 2028 (1993).
[11] A.J. Koning and J.M. Akkermans, Ann. Phys. (N.Y.) **208**, 216 (1991).
[12] T. Tamura, T. Udagawa, and H. Lenske, Phys. Rev. C **26**, 379 (1982).
[13] H. Nishioka, H.A. Weidenmuller, and S. Yoshida, Ann. Phys. (N.Y.) **172**, 67 (1986).
[14] F.C. Williams, Nucl. Phys. **A166**, 231 (1971).
[15] W. Dilg, W. Schantl, H. Vonach, and M. Uhl, Nucl. Phys. **A217**, 269 (1973).
[16] H. Gruppelaar, *IAEA Advisory Group Meeting on Basic and Applied Problems on Nuclear Level Densities* (Brookhaven National Laboratory, 1983).
[17] P.A. Seeger and R.C. Perisho, Los Alamos Report No. LA-3751, 1967.
[18] H. Feshbach, Ann. Phys. (N.Y.) **159**, 150 (1985).
[19] R. Bonetti, M. Camnasio, L. Colli Milazzo, and P.E. Hodgson, Phys. Rev. C **24**, 71 (1981).
[20] A. Marcinkowski, R.W. Finlay, J. Rapaport, P.E. Hodgson, and M.B. Chadwick, Nucl. Phys. **A501**, 1 (1989).
[21] P.D. Kunz, DWUCK4 code, University of Colorado (unpublished).
[22] M.B. Chadwick, Ph.D. thesis, Oxford University, 1989.
[23] M.B. Chadwick, R. Bonetti, and P.E. Hodgson, J. Phys. G **15**, 1689 (1989).
[24] P. Oblozinsky and M.B. Chadwick, Phys. Rev. C **42**, 1652 (1990).
[25] P.G. Young, E.D. Arthur, and M.B. Chadwick, Los Alamos National Laboratory Report No. LA-12343-MS, 1992.
[26] E. Gadioli and P.E. Hodgson, *Preequilibrium Nuclear Reactions* (Oxford University Press, New York, 1992).
[27] M. Herman (private communication).
[28] H. Nishioka, H.A. Weidenmuller, and S. Yoshida, Z. Phys. A **336**, 197 (1990).
[29] C. Kalbach, Phys. Rev. C **37**, 2350 (1988).
[30] H. Kalka, M. Torjman, and D. Seeliger, Phys. Rev. C

40, 1619 (1989).
[31] H. Gruppelaar and P. Nagel, "International Nuclear Model and Code Comparison on Preequilibrium Effects," Newsletter No. 32 of the Nuclear Energy Agency Data Bank, NEANDC-204 'U' (Gif-sur-Yvette, France, 1985).
[32] D. Wilmore and P.E. Hodgson, Nucl. Phys. **55**, 673 (1964).
[33] F.D. Becchetti, Jr. and G.W. Greenlees, Phys. Rev. **182**, 1190 (1969).
[34] A. Pavlik, A. Priller, and H. Vonach, in *Proceedings of the Final Research Coordination Meeting (RCM-3) of the Co-ordinated Research Programme (CRP) on Measurements and Analysis of 14 MeV Neutron-Induced Double Differential Neutron Emission Cross Sections needed for Fission and Fusion Reactor Technology*, Chiang Mai, 1992 (International Atomic Energy Agency, Vienna, in press).
[35] R. Fischer, M. Uhl, and H. Vonach, Phys. Rev. C **37**, 578 (1988).
[36] A. Takahashi *et al.*, Oktavian Report No. A-92-01, 1992.
[37] A. Marcinkowski *et al.*, Nucl. Sci. Eng. **83**, 13 (1983).
[38] A. Koning, in *Proceedings of the Symposium on Nuclear Data Evaluation Methodology*, Brookhaven National Laboratory, Upton, New York, 1992, edited by C. Dunford (World Scientific, Singapore, in press).
[39] K. Kalbach-Cline, Nucl. Phys. **A210**, 590 (1973).
[40] R. Bonetti, L. Colli Milazzo, and M. Melanotte, Phys. Rev. C **27**, 1003 (1983).